

## Article

# Naphth[1,2-*d*]imidazoles Bioactive from $\beta$ -Lapachone: Fluorescent Probes and Cytotoxic Agents to Cancer Cells

Victória Laysna dos Anjos Santos <sup>1</sup>, Arlan de Assis Gonsalves <sup>1,2</sup>, Délis Galvão Guimarães <sup>3</sup>, Sidney Silva Simplicio <sup>1</sup> , Helinando Pequeno de Oliveira <sup>2</sup> , Lara Polyana Silva Ramos <sup>4</sup>, Marcília Pinheiro da Costa <sup>4</sup> , Fátima de Cássia Evangelista de Oliveira <sup>5</sup> , Claudia Pessoa <sup>5</sup>  and Cleônia Roberta Melo Araújo <sup>1,\*</sup> 

- <sup>1</sup> Graduate Program in Health and Biological Sciences, Universidade Federal do Vale do São Francisco, Av. José de Sá Maniçoba s/n, Campus Centro, Petrolina 56304-917, Brazil; victoria.laysna@univasf.edu.br (V.L.d.A.S.); arlan.gonsalves@univasf.edu.br (A.d.A.G.); sidney.simplicio@discente.univasf.edu.br (S.S.S.)
  - <sup>2</sup> Graduate Program in Materials Science, Universidade Federal do Vale do São Francisco, Av. Antônio Carlos Magalhães 510, Campus Juazeiro, Juazeiro 48902-300, Brazil; helinando.oliveira@univasf.edu.br
  - <sup>3</sup> Graduate Program in Biotechnology, Rede Nordeste de Biotecnologia—RENORBIO, Centro de Biociências, Universidade Federal do Rio Grande do Norte, Campus Lagoa Nova, Natal 59078-900, Brazil; delisgalvao@gmail.com
  - <sup>4</sup> Graduate Program in Pharmaceutical Sciences, Universidade Federal do Piauí, Teresina 64049-550, Brazil; lara\_poliana@hotmail.com (L.P.S.R.)
  - <sup>5</sup> Graduate Program in Physiology and Pharmacology, Universidade Federal do Ceará, Fortaleza 60430-270, Brazil; cassiadefatima3006@gmail.com (F.d.C.E.d.O.); cpessoa@ufc.br (C.P.)
- \* Correspondence: cleonia.araujo@univasf.edu.br

**Abstract:** Theranostics combines therapeutic and imaging diagnostic techniques that are extremely dependent on the action of imaging agent, transporter of therapeutic molecules, and specific target ligand, in which fluorescent probes can act as diagnostic agents. In particular, naphthoimidazoles are potential bioactive heterocycle compounds to be used in several biomedical applications. With this aim, a group of seven naphth[1,2-*d*]imidazole compounds were synthesized from  $\beta$ -lapachone. Their optical properties and their cytotoxic activity against cancer cells and their compounds were evaluated and confirmed promising values for molar absorptivity coefficients (on the order of  $10^3$  to  $10^4$ ), intense fluorescence emissions in the blue region, and large Stokes shifts (20–103 nm). Furthermore, the probes were also selective for analyzed cancer cells (leukemic cells (HL-60)). The naphth[1,2-*d*]imidazoles showed  $IC_{50}$  between 8.71 and 29.92  $\mu$ M against HL-60 cells. For HCT-116 cells, values for  $IC_{50}$  between 21.12 and 62.11  $\mu$ M were observed. The selective cytotoxicity towards cancer cells and the fluorescence of the synthesized naphth[1,2-*d*]imidazoles are promising responses that make possible the application of these components in antitumor theranostic systems.

**Keywords:** heterocycle; anticancer; fluorescent probe; theranostic; naphthoimidazole



**Citation:** Santos, V.L.d.A.; Gonsalves, A.d.A.; Guimarães, D.G.; Simplicio, S.S.; Oliveira, H.P.d.; Ramos, L.P.S.; Costa, M.P.d.; Oliveira, F.d.C.E.d.; Pessoa, C.; Araújo, C.R.M. Naphth[1,2-*d*]imidazoles Bioactive from  $\beta$ -Lapachone: Fluorescent Probes and Cytotoxic Agents to Cancer Cells. *Molecules* **2023**, *28*, 3008. <https://doi.org/10.3390/molecules28073008>

Academic Editors: Edward Krzyżak, Piotr Świątek and Dominika Szkatuła

Received: 23 February 2023

Revised: 16 March 2023

Accepted: 18 March 2023

Published: 28 March 2023



**Copyright:** © 2023 by the authors. Licensee MDPI, Basel, Switzerland. This article is an open access article distributed under the terms and conditions of the Creative Commons Attribution (CC BY) license (<https://creativecommons.org/licenses/by/4.0/>).

## 1. Introduction

The multifunctionality of theranostic agents introduces several advantages for medicine, overcoming pharmacokinetic and selectivity issues of conventional therapy and diagnostic agents [1], while providing the image monitoring of pathology progression as well as the pharmacokinetic profile of the drug in the body [2].

The design of a theranostic agent requires a combination of different areas, such as chemistry, physics, nanotechnology, biochemistry, and engineering, with the aim of obtaining a multifunctional platform capable of performing non-invasive therapy and diagnosis of a pathological condition [3]. Typically, a theranostic agent is composed of (i) an imaging agent, (ii) a therapeutic molecule, (iii) a target-specific ligand, and (iv) a carrier. The diagnostic agent is a fundamental part of a theranostic system. It favors the non-invasive visualization of cellular and subcellular processes of a pathological condition

through image emission. Examples of these components include fluorophores with the ability to respond to specific stimuli regarding the identification of biological species [4,5].

Fluorescent compounds, such as naphthoxazoles, have been explored as active molecules in biological systems [6]. Imidazoles and oxazoles can be synthesized through a multicomponent reaction, the Debus–Radziszewski reaction, employing  $\alpha$ -dicarbonyl compounds and aldehydes [7,8]. The same reaction generates naphthoimidazoles and naphthoxazoles in which 1,2-naphthoquinones are used as  $\alpha$ -dicarbonyl compounds [9,10].  $\beta$ -Lapachone is a 1,2-naphthoquinone originally isolated from the heartwood of *Handroanthus impetiginosus* [11], which can be considered a potential antitumor agent [12–14]. The efficacy of  $\beta$ -lapachone for cancer treatment was evaluated through phase I and II clinical trials, with the naphthoquinone in the form of ARQ 501 and ARQ 761 [15–18]. However, several drawbacks of  $\beta$ -lapachone, such as low water solubility and narrow therapeutic windows, limited its clinical applications [19,20].

Based on the cytotoxicity of  $\beta$ -lapachone and the fluorescent properties of naphthoazole heterocycles, the scaffold 1,2-naphtho[1,2-*d*]imidazole was designed to be a fluorescent emitter with antitumor action, being considered a promising component of theranostic systems, as shown in Figure 1.

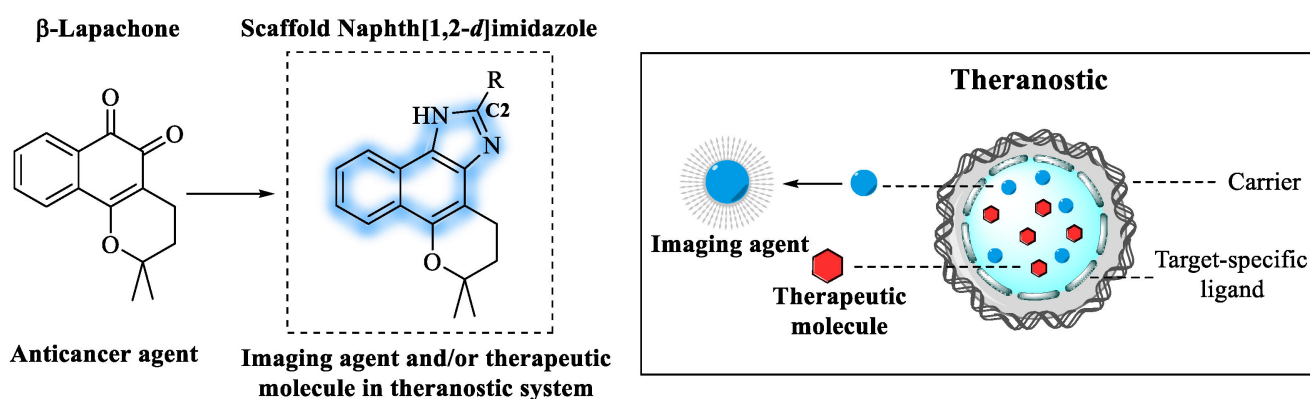
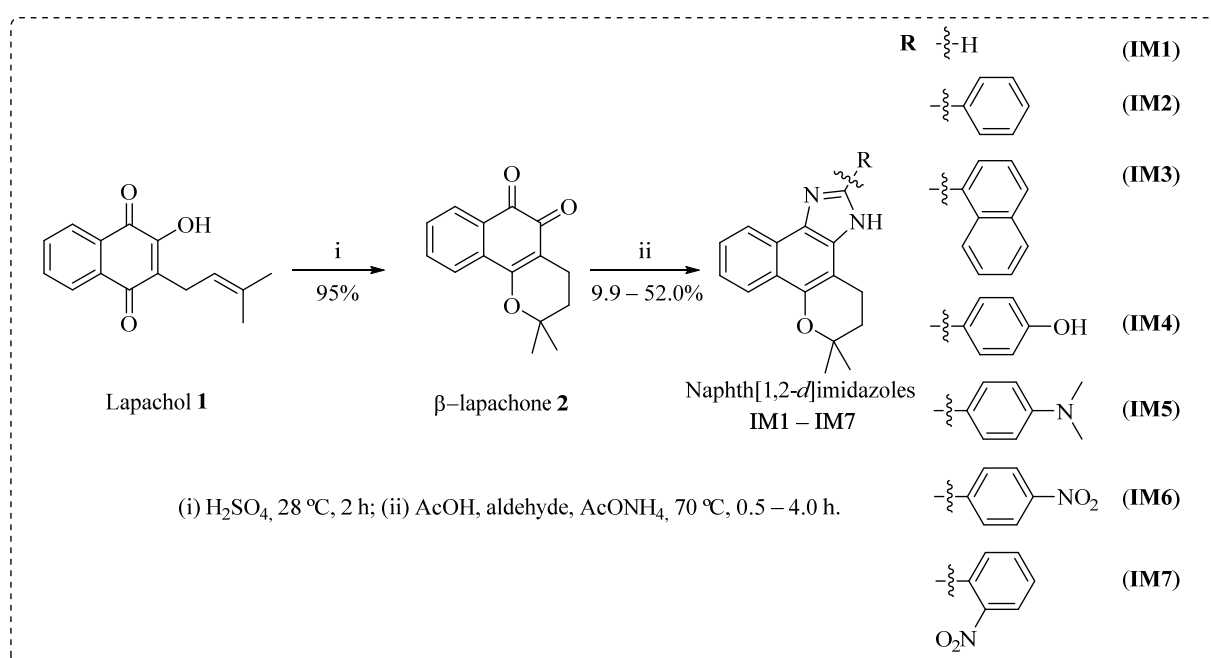


**Figure 1.** Molecular design of the naphth[1,2-*d*]imidazoles with anticancer and fluorescent properties.

Herein, it is reported the synthesis of different naphth[1,2-*d*]imidazoles, with modification of substituents at the C2 position of the naphthoimidazole ring, and the following evaluation of their photophysical and anticancer activity as a part of a strategy to provide a new class of materials with promising biomedical applicability.

## 2. Results and Discussion

Naphth[1,2-*d*]imidazoles **IM1–IM7** were prepared in two steps (Scheme 1) from lapachol **1**, in which the natural 1,4-naphthoquinone was extracted from the heartwood of trees of the genus *Tabebuia*. In the first step,  $\beta$ -lapachone ( $\beta$ -Lap **2**) was obtained from the acid-catalyzed cyclization of lapachol **1** using sulfuric acid ( $\text{H}_2\text{SO}_4$ ). In the following step, the compounds **IM1–IM7** were synthesized through the Debus–Radziszewski reaction, in a one-pot process between  $\beta$ -Lap **2** and the corresponding aldehyde, using ammonium acetate as a source of ammonia (Scheme 1). The reactions were established at 70 °C in acetic acid with a reaction time range of 0.5–4.0 h. The crude reactions were treated with sodium bisulfite ( $\text{NaHSO}_3$ ), and the products were purified using column chromatography or recrystallization. The naphthoimidazoles returned yields in the range of 9.9 to 52.0%, and their structures were scrutinized by analyzing the 1D and 2D Nuclear Magnetic Resonance (NMR) spectra, mass spectroscopy, and Fourier Transform Infrared (FTIR).



**Scheme 1.** Synthetic route to obtain the naphth[1,2-*d*]imidazoles **IM1–IM7**.

### 2.1. Optical Properties—Studies of Absorption and Fluorescence Spectra

Fluorescent molecules with the ability to absorb ultraviolet radiation and to emit in a range of wavelengths greater than that absorbed, that is, in the visible region, are extremely important to biomedical applications [21]. The characteristic time for the fluorescence process (on the order of  $10^{-9}$  s) depends on the interaction of molecules with the surrounding environment, being attractive for the evaluation of several phenomena from the biophysical properties of molecules [21]. Thus, the photophysical study of the naphth[1,2-*d*]imidazoles **IM1–IM7** synthesized was carried out to verify their potential to emission of molecules for potential use in theranostic systems. The data for Ultraviolet–visible (UV–vis) absorption and fluorescence spectroscopy from naphth[1,2-*d*]imidazoles **IM1–IM7** are summarized in Table 1.

#### 2.1.1. Solvatochromism Study

The dispersed molecules in a specific solvent can interact with other molecules of a fluorophore, affecting their emissive properties [22]. This phenomenon is called solvatochromism and depends on factors such as the polarity of the solvent, hydrogen bonding ability, pH, and viscosity of the solvent [22,23]. Considering the application of fluorescent probes in living cells and tissues, the solvatochromism study can evaluate the sensitivity and selectivity of the new compounds [24].

The influence of the solvent on optical characteristics of the synthesized naphth[1,2-*d*]imidazoles **IM1–IM7** was evaluated from the solvatochromism study that considered four solvents: hexane, dichloromethane ( $\text{CH}_2\text{Cl}_2$ ), dimethyl sulfoxide (DMSO), and methanol ( $\text{CH}_3\text{OH}$ ) (Table S1). From the UV–vis absorption spectra of the naphth[1,2-*d*]imidazoles (for different solvents), it was possible to determine the most suitable solvents and wavelengths for further photophysical studies. The criteria considered solvents for naphth[1,2-*d*]imidazoles that presented positive solvatochromism, i.e., redshift with increasing polarity of the solvent.

The absorption spectra of 2-substituted naphth[1,2-*d*]imidazoles (**IM2–IM7**) showed two absorption bands in the ultraviolet region, corresponding to the  $\pi \rightarrow \pi^*$  transition of the substituent at the carbon C2 of the naphthimidazole ring ( $\sim 314$  nm) and of the imidazole ring ( $\sim 363$  nm) [25–27] (Table S1).

The naphth[1,2-*d*]imidazoles **IM2** and **IM6** showed a higher bathochromic shift for polar solvents, a strong influence of the increasing solvent polarity on the absorption spectrum of these derivatives. On the other hand, **IM7** showed a positive bathochromic effect in comparison to hexane, a nonpolar solvent. The other naphthoimidazoles (**IM1**, **IM3**, **IM4**, and **IM5**) exhibited an increasing redshift in CH<sub>2</sub>Cl<sub>2</sub> (Table S1).

### 2.1.2. Molar Absorption Coefficient

The molar absorption coefficient ( $\epsilon_{\text{Abs}}$ ) is also an important parameter for the development of fluorescent probes. Samples prepared with naphth[1,2-*d*]imidazoles **IM1–IM7** showed high  $\epsilon_{\text{Abs}}$  on the order of  $10^3$  to  $10^4$  M<sup>-1</sup> cm<sup>-1</sup> (Table 1), which is consistent with the allowed transition  $\pi \rightarrow \pi^*$  of  $\pi$ -conjugated systems [26,28–30] characteristic of the imidazole nucleus [25,31].

**Table 1.** Photophysical properties of the naphth[1,2-*d*]imidazoles **IM1–IM7**.

Compound	Solvent	$\lambda_{\text{max}}$ (nm)	$\epsilon_{\text{Abs}}^{\text{a}}$ ( $10^4$ M <sup>-1</sup> cm <sup>-1</sup> )	$\lambda_{\text{emis}}^{\text{b}}$ (nm)	$\Delta\text{ST}^{\text{c}}$ (nm)
<b>IM1</b>	CH <sub>2</sub> Cl <sub>2</sub>	316	0.61	366	50
<b>IM2</b>	DMSO	342	2.43	402	60
<b>IM3</b>	CH <sub>2</sub> Cl <sub>2</sub>	354	1.57	457	103
<b>IM4</b>	CH <sub>2</sub> Cl <sub>2</sub>	344	1.48	393	49
<b>IM5</b>	CH <sub>2</sub> Cl <sub>2</sub>	368	2.71	422	54
<b>IM6</b>	CH <sub>3</sub> OH	411	1.85	391	20
<b>IM7</b>	Hexane	337	1.35	385	48
DAPI	H <sub>2</sub> O	343 <sup>d</sup>	-	452	112

<sup>a</sup>: Molar absorptivity coefficient at the concentration of 20  $\mu\text{M}$ . <sup>b</sup>: Emission wavelength after excitation at 345 nm. <sup>c</sup>: Stokes shift. <sup>d</sup>: Data obtained from Farahat et al. (2017) [32].

### 2.1.3. Fluorescence Spectroscopy Experiments

Considering the UV–vis absorption spectra of the naphth[1,2-*d*]imidazoles **IM1–IM7**, the excitation wavelength of 345 nm was chosen to obtain the fluorescence spectra. Analyzing the fluorescence emission spectra of compounds **IM1–IM7**, the emission was observed in the UV–vis region, between the  $\lambda_{\text{emis}}$  values of 366 and 457 nm (Figure 2). **IM3** ( $\lambda_{\text{emis}}$  457 nm) and **IM5** ( $\lambda_{\text{emis}}$  422 nm), emitted at lower energy wavelengths, shifted more to the blue region. On the other hand, **IM1**, emitted at a higher energy wavelength, shifted toward the violet region (Figure 2).

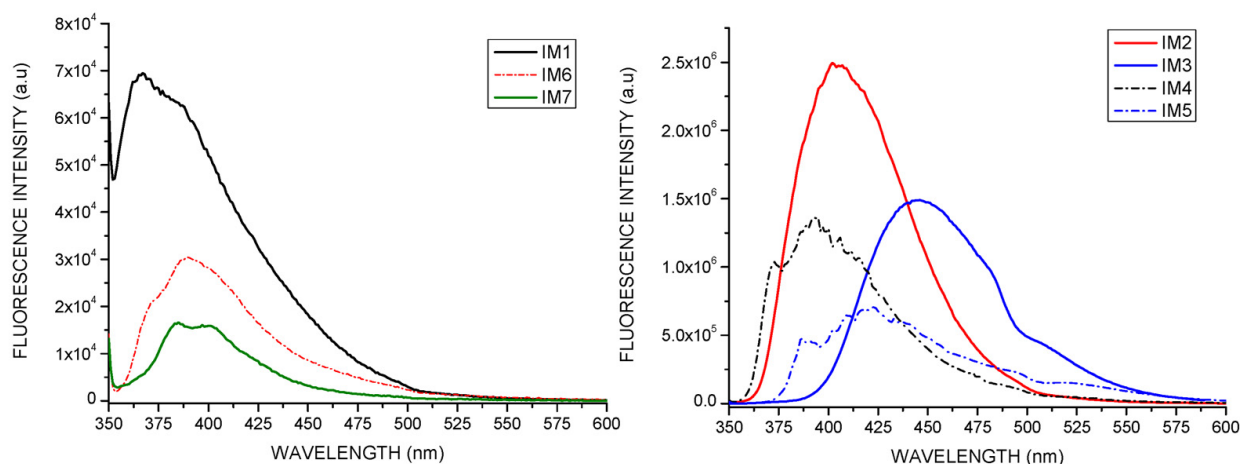


**Figure 2.** Fluorescence emission spectra of the synthesized naphth[1,2-*d*]imidazoles ( $\lambda_{\text{Exc}}$  345 nm).

In addition, **IM2** ( $2.49 \times 10^6$  au) and **IM3** ( $1.41 \times 10^6$  au) showed fluorescence emission intensities that were thirty-six and twenty-three times greater, respectively, than **IM1**

( $6.90 \times 10^4$  au), indicating that the substitution at the carbon C2 of the naphthoimidazole ring favored the fluorescence emission of naphth[1,2-*d*]imidazoles **IM1–IM7** (Figure 2). The increase in the fluorescence evaluated by the substitution of the carbon C2 position is due to the increase in the conjugation of double bonds, providing more-effective intramolecular displacement of electrons [25,33].

By comparison between the fluorescence of **IM4**, **IM5**, and **IM6**, a positive influence on fluorescence was observed in compounds containing electron-donor substituents in the aromatic ring located at C2 of the naphth[1,2-*d*]imidazoles with **IM4** and **IM5** substituted with 4-hydroxyphenyl and 4-dimethylaminophenyl, respectively, showing higher fluorescence intensity than **IM6**, substituted with 4-nitrophenyl. The higher fluorescence of **IM4** and **IM5**, if compared with other fluorophores, is attributed to a possible intramolecular charge transfer (ICT) [34].

Considering the fluorescence intensity emitted, the **IM2**, followed by the **IM3**, **IM4**, and **IM5** compounds, showed the best results. All samples presented higher fluorescence than that observed for the 4',6-diamidino-2-phenylindole (DAPI), the fluorescent DNA marker [35].

DAPI exhibits photophysical characteristics of absorption and emission ( $\lambda_{\text{abs}}$  340 nm and  $\lambda_{\text{emis}}$  453–461 nm) similar to the synthesized naphth[1,2-*d*]imidazoles. By comparison of the fluorescence emission of DAPI ( $1.13 \times 10^5$  au) to that of **IM2** ( $2.49 \times 10^6$  au), **IM3** ( $1.41 \times 10^6$  au), **IM4** ( $1.36 \times 10^6$  au), and **IM5** ( $7.04 \times 10^5$  au), it was observed that IM compounds also present more intense fluorescence in the blue region than DAPI. This may be due to the extension of the conjugated double-bond system of the synthesized naphth[1,2-*d*]imidazoles enhanced by the presence of the naphthalene system associated with the 2-substituted imidazole (Figure 3).

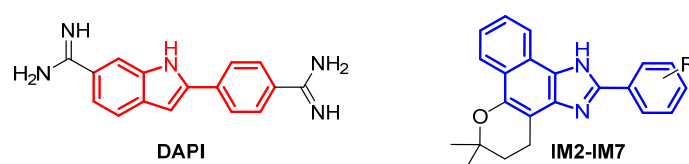


**Figure 3.** Structural similarity of DAPI and synthesized naphth[1,2-*d*]imidazoles.

#### 2.1.4. Stokes Shift

Fluorophores with large Stokes shifts ( $\Delta_{\text{ST}}$ ) are considered promising fluorescent probes for application in vivo cell-imaging studies, since they could minimize the background fluorescence in live tissues [36–40]. The naphth[1,2-*d*]imidazoles **IM1–IM7** presented  $\Delta_{\text{ST}}$  between 20 and 103 nm (Table 2). If compared with the structure and  $\Delta_{\text{ST}}$  of naphth[1,2-*d*]imidazoles **IM1–IM7**, it was observed that the substituents at C2 affect the ability of this compound to be a fluorophore. **IM1** has no substituents on C2 and was the one with the smallest  $\Delta_{\text{ST}}$ , as well as the lowest fluorescence emission ( $6.90 \times 10^4$  au). **IM3** presented the largest displacement, which is substituted at C2 with a naphthyl group. It was also observed that the introduction of electron-withdrawing substituents, such as nitrophenyl, produced naphthoimidazoles with narrow  $\Delta_{\text{ST}}$ , as shown for **IM6** ( $\Delta_{\text{ST}}$  20 nm) and **IM7** ( $\Delta_{\text{ST}}$  48 nm).

#### 2.2. Cytotoxicity Assay

The cytotoxic activity of the naphth[1,2-*d*]imidazoles **IM1–IM7** was assessed through colorimetric MTT assay [41,42]. The ability of these compounds to inhibit cell growth against human glioblastoma (SNB-19), human colorectal carcinoma (HCT-116), and human promyelocytic leukemia (HL-60) cell lines was evaluated. The  $\text{IC}_{50}$  was determined for those compounds, returning a percentage inhibition of cell growth above 75% in at least two tested cell lines. Thus, from all seven naphth[1,2-*d*]imidazoles tested (**IM1–IM7**), only **IM3** displayed low growth inhibition against all cell lines and did not have the  $\text{IC}_{50}$  calculated due to low cytotoxic activity. Doxorubicin was used as the positive control, and

cytotoxic activities were expressed as IC<sub>50</sub> for all the naphth[1,2-*d*]imidazoles in Table 2. The substances that displayed significant results against the cancer cell lines were also investigated against a nontumor cell line of murine fibroblast (L929) to evaluate their selectivity index (SI) (Table 2).

**Table 2.** Cytotoxic activity of **IM1**, **IM2**, **IM4**, **IM5**, **IM6**, and **IM7** after a 72 h exposure expressed by IC<sub>50</sub> (μM) and confidence interval.

Compound	Cell Line						
	L929	SNB-19		HCT-116		HL-60	
	IC <sub>50</sub> (μM) <sup>a</sup>	IC <sub>50</sub> (μM) <sup>a</sup>	SI <sup>b</sup>	IC <sub>50</sub> (μM) <sup>a</sup>	SI <sup>b</sup>	IC <sub>50</sub> (μM) <sup>a</sup>	SI <sup>b</sup>
<b>IM1</b>	186.17	46.44 (38.59–55.76)	4.00	62.11 (54.14–71.31)	3.00	24.23 (22.32–21.41)	7.68
<b>IM2</b>	104.85	26.97 (24.44–26.96)	3.89	21.69 (18.34–25.66)	4.83	29.92 (14.44–19.87)	3.50
<b>IM4</b>	>363.21	31.90 (28.39–35.83)	>11.38	23.04 (21.56–24.67)	>15.76	8.71 (7.46–10.22)	>41.70
<b>IM5</b>	52.84	21.05 (18.20–24.39)	2.51	44.07 (37.42–51.87)	1.20	12.35 (10.22–14.55)	4.28
<b>IM6</b>	151.55	22.27 (20.23–24.49)	6.81	21.12 (19.56–22.78)	7.18	13.67 (14.79–18.09)	11.09
<b>IM7</b>	NE	>67.00	NE	35.11 (28.94–42.56)	NE	14.90 (10.64–14.17)	NE
Doxorubicin	3.16	2.21 (1.90–2.56)	1.43	0.20 (0.15–0.26)	15.80	0.04 (0.035–0.039)	79.00

NE—not evaluated. <sup>a</sup>: IC<sub>50</sub> is the concentration at which 50% of cells were undergoing cytotoxic cell death due to synthesized compound treatment. <sup>b</sup>: SI (selectivity index) equals the ratio of IC<sub>50</sub> for fibroblasts L929/IC<sub>50</sub> for the cancer cell lines.

As shown in Table 2, most of the naphth[1,2-*d*]imidazoles are characterized by a certain degree of cytotoxicity against at least one of the malignant cell lines tested. The IC<sub>50</sub> data showed that **IM1** was the least potent imidazole of the series, demonstrating the importance of the substitution at the C2 carbon of the naphth[1,2-*d*]imidazole ring for the cytotoxic activity against the tested cancer cell lines. If considering the comparison of the influence of substituents at the C2 position, a significant decrease in cell growth inhibition was observed for naphthoimidazole with a naphthyl ring at C2 (**IM3**), suggesting that the phenyl substituent at the C2 position of the naphthoimidazole ring is relevant for the evaluated activity.

Against glioblastoma cells (SNB-19), the most cytotoxic compound was **IM5** (IC<sub>50</sub> 21.05 μM). As for HCT-116 cells and leukemia cells (HL-60), the most active naphth[1,2-*d*]imidazoles were **IM6** and **IM4**, with IC<sub>50</sub> of 21.12 and 8.71 μM, respectively. Comparing the three most cytotoxic imidazoles (**IM4**, **IM5**, and **IM6**) for each cancer cell line tested, it was observed that all of them presented as a substituent at the C2 position a 4-substituted phenyl ring with an electronegative group: -OH, -N(CH<sub>3</sub>)<sub>2</sub>, and NO<sub>2</sub>, respectively. Thus, it is possible to suggest that the substituted phenyl group located at the C2 carbon of the naphthoimidazole ring improves cytotoxicity activity and promotes selectivity.

In addition, for the cytotoxic activity of **IM6** and **IM7** (Table 2) for each cancer cell line tested, it can be seen that the 2-nitrophenyl substituent group at the C2 carbon of the naphthoimidazole ring makes the compound less cytotoxic to the evaluated tumor cell lines. Comparing the cytotoxic activity against three cancer cell lines, the tested naphthoimidazoles showed to be more active against the leukemia cell line (HL-60), presenting IC<sub>50</sub> between 8.71 and 29.92 μM. Among them, **IM4** was the most active compound, with an emphasis on its high selectivity for leukemic cells (SI > 41.67).

By considering that high  $\epsilon_{\text{Abs}}$  values combined with large  $\Delta_{\text{ST}}$  are desirable for fluorescent probes [43] and the photophysical and cytotoxic properties of each naphth[1,2-*d*]imidazole, one can infer that **IM3** (fluorescence intensity  $1.41 \times 10^6$  au,  $\epsilon_{\text{Abs}}$   $1.57 \times 10^4 \text{ M}^{-1} \text{ cm}^{-1}$  and  $\Delta_{\text{ST}}$  103 nm) fits as a good fluorescent probe; however, it showed low cytotoxicity on the cell lines tested. One can also infer that **IM2** (fluorescence intensity  $2.49 \times 10^6$  au;  $\epsilon_{\text{Abs}}$   $2.43 \times 10^4 \text{ M}^{-1} \text{ cm}^{-1}$  and  $\Delta_{\text{ST}}$  60 nm) has photophysical properties that qualify it as a fluorescent probe, and it has cytotoxicity against HCT-116 ( $\text{IC}_{50}$  21.69  $\mu\text{M}$ ) and selectivity (SI 4.83).

**IM4** stands out for cytotoxicity against HL-60 ( $\text{IC}_{50}$  8.71  $\mu\text{M}$ ) and selectivity (SI > 41.70); at the same time, it appears to have a high intensity of fluorescence ( $1.36 \times 10^6$  au) and moderate  $\epsilon_{\text{Abs}}$  ( $1.48 \times 10^4 \text{ M}^{-1} \text{ cm}^{-1}$ ) and  $\Delta_{\text{ST}}$  49 nm. **IM5** was cytotoxic to SNB-19 ( $\text{IC}_{50}$  21.05  $\mu\text{M}$  and SI 2.51) and showed promising photophysical properties (fluorescence  $7.04 \times 10^5$  au;  $\epsilon_{\text{Abs}}$   $2.71 \times 10^4 \text{ M}^{-1} \text{ cm}^{-1}$  and  $\Delta_{\text{ST}}$  54 nm).

### 3. Materials and Methods

#### 3.1. Materials

All chemicals were purchased from commercial suppliers and used without further purification. Melting points were determined through a PFM-II (Instrumentation MS Tecnopon<sup>®</sup>) melting-point apparatus. The purity of the compounds synthesized was determined by thin-layer chromatography (TLC) using several solvent systems of different polarities. Purification of these compounds was done by column chromatography. Infrared (IR) spectra were recorded on a PerkinElmer (model 10.4.00) spectrophotometer equipped with an Attenuated Total Reflectance ATR sampling unit. NMR spectra were recorded on a Bruker Ascend 400 spectrometer, operating at 400 MHz for  $^1\text{H}$  NMR and 100 MHz for  $^{13}\text{C}$  NMR.  $\text{CDCl}_3$  and  $\text{DMSO-d}_6$  were used as solvents with tetramethylsilane (TMS) as the internal standard; chemical shifts ( $\delta$ ) are given in ppm and coupling constants (J) in Hz. Mass spectra were recorded with a Bruker Daltonics (TOF-Q-II) spectrometer using electrospray ionization. UV-vis absorption spectra were obtained using a Hach/Lange spectrophotometer (model DR 5000). Fluorescence emission spectra were obtained using the ISS spectrofluorometer (model PC1).

#### 3.2. Synthesis of Naphth[1,2-*d*]imidazoles **IM1–IM7**

##### 3.2.1. Synthesis of $\beta$ -Lapachone 2

Lapachol **1** was extracted from the wood of a plant of the genus *Tabebuia* and used after purification and identification, as described previously [44]. The access was registered in the National System of Genetic Heritage and Associated Traditional Knowledge (SISGEN) under the A5FDA89. Yield: 1.5% (m/m). Yellow solid, mp: 138.3–140.3 °C (Lit 139.0–141.0 °C) [45].

In a 25 mL reaction flask, the lapachol (484 mg, 2 mmol) was weighed and incorporated into a concentrated sulfuric acid ( $\text{H}_2\text{SO}_4$ ) solution (5 mL). The reaction mixture was stirred at room temperature for 1.0 h, then poured into 400 mL of ice-cold deionized water. The solid obtained was vacuum filtered and allowed to dry at room temperature [44], which resulted in a yield of 95%. Orange solid, mp: 155 °C (Lit 154–155 °C) [46].  $^1\text{H}$  NMR (400 MHz,  $\text{DMSO-d}_6$ )  $\delta$  [ppm]: 7.91 (d,  $J = 7.6$  Hz, 1H), 7.77 (m, 2H), 7.61 (m, 1H), 2.40 (t,  $J = 6.6$  Hz, 2H), 1.82 (t,  $J = 6.6$  Hz, 2H), 1.43 (s, 6H).  $^{13}\text{C}$  NMR (100 MHz  $\text{DMSO-d}_6$ )  $\delta$  (ppm): 179.1, 177.8, 160.6, 135.0, 132.1, 130.8, 129.9, 127.8, 123.7, 112.5, 79.0, 30.8, 26.3, 15.9.

##### 3.2.2. General Synthesis of the Naphth[1,2-*d*]imidazoles

The solution of  $\beta$ -Lap **2** (242 mg; 1.0 mmol) was prepared in glacial acetic acid (6 mL), and was added aldehyde adequate (2.5 mmol). The reaction mixture was placed at a temperature of 70 °C and added to ammonium acetate (1.27 g; 16.5 mmol) that was divided into three parts and remained at this temperature under stirring until the end of the reaction [10]. The reactions were followed by Thin Layer Chromatography (TLC), and the reaction times varied in the range of 30 min to 4 h. In experiments using 4-

dimethylaminobenzaldehyde and 4-nitrobenzaldehyde, there was a precipitate formation in the reaction. However, in experiments employing formaldehyde, benzaldehyde, 1-naphthaldehyde, 4-hydroxybenzaldehyde, and 2-nitrobenzaldehyde, there was no precipitate formation in the reaction. Then, after the reaction time, the reaction mixture was poured into a cold solution of 5.0% (*m/v*) of NaHSO<sub>3</sub> for precipitate formation. The solid was filtered and washed with a solution of 5.0% (*m/v*) of NaHCO<sub>3</sub>, and water was deionized at neutral pH and dried at room temperature.

#### Synthesis of 4,5-dihydro-6,6-dimethyl-6*H*-2-pyran[*b*-4,3]naphth[1,2-*d*]imidazole (**IM1**)

The reaction was heated to 70 °C for 4.0 h. Compound **IM1** was obtained as a yellow crystalline solid (131 mg, 0.519 mmol, yield: 52.0%), mp: 255–259 °C. <sup>1</sup>H NMR (400 MHz, DMSO-*d*<sub>6</sub>) δ [ppm]: 8.30 (d, *J* = 8.0 Hz, 1H), 8.17 (s, 1H), 8.12 (d, 1H), 7.54 (t, 1H), 7.42 (t, 1H), 2.98 (t, 2H), 1.94 (t, 2H), 1.40 (s, 6H). <sup>13</sup>C NMR (100 MHz, DMSO-*d*<sub>6</sub>) δ [ppm]: 143.9, 132.9, 138.4, 127.7, 125.7, 124.1, 123.3, 122.7, 122.1, 121.0, 104.4, 74.2, 31.5, 26.5, 18.5. IR (KBr)  $\nu_{\max}/\text{cm}^{-1}$ : 3435, 3088, 2971, 2925, 2841, 1608, 1538, 1484, 1453, 1362, 1252, 1164, 1122, 1054, 947, and 770, Figure S1.

#### Synthesis of 4,5-dihydro-6,6-dimethyl-6*H*-2-(phenyl)-pyran[*b*-4,3]naphth[1,2-*d*]imidazole (**IM2**)

The reaction was heated to 70 °C for 1.0 h. Compound **IM2** was obtained as a light-yellow solid (60 mg, 0.183 mmol, yield: 18.3%), mp: 278–279 °C. <sup>1</sup>H NMR (400 MHz, DMSO-*d*<sub>6</sub>) δ [ppm]: 13.24 (s, 0.3H), 12.76 (s, 0.5H), 8.37–8.46 (m, 1H), 8.20–8.29 (m, 2H), 8.10–8.20 (m, 1H), 7.51–7.63 (m, 3H), 7.39–7.51 (m, 2H), 3.00–3.17 (m, 2H), 1.87–2.06 (m, 2H), 1.43 (s, 6H). <sup>13</sup>C NMR (100 MHz, DMSO-*d*<sub>6</sub>) δ [ppm]: 147.9, 144.5, 132.2, 131.2, 130.6, 129.1, 128.8, 126.0, 125.9, 125.7, 123.4, 122.8, 122.1, 121.2, 102.4, 74.4, 31.4, 26.5, 18.8. IR (KBr)  $\nu_{\max}/\text{cm}^{-1}$ : 3432, 3067, 2972, 2852, 2928, 1600, 1520, 1256, 1157, and 1056. HRMS (ESI-TOF) calculated for C<sub>22</sub>H<sub>20</sub>N<sub>2</sub>O [M+H]<sup>+</sup>: 329.1609. Found: 329.1646, Figure S2.

#### Synthesis of 4,5-dihydro-6,6-dimethyl-6*H*-2-(naphthalenyl)-pyran[*b*-4,3]naphth[1,2-*d*]imidazole (**IM3**)

The reaction was heated to 70 °C for 2.0 h. Compound **IM3** was obtained as a pale-yellow solid (83 mg, 0.22 mmol, yield: 25.4%). <sup>1</sup>H NMR (400 MHz, DMSO-*d*<sub>6</sub>) δ [ppm]: 13.39 (s, 0.4H); 12.92 (s, 0.6H); 9.15 (dd, 1H); 8.45 (dd, 1H); 8.19 (d, *J* = 7.9 Hz, 1H); 8.02–8.12 (m, 3H); 7.55–7.74 (m, 4H); 7.41–7.49 (m, 1H); 3.06 (m, 1.2H); 3.18 (m, 0.8H); 2.00 (m, 2H); 1.45 (s, 6H). <sup>13</sup>C NMR (100 MHz, DMSO-*d*<sub>6</sub>) δ [ppm]: 147.7, 144.5, 133.6, 132.2, 130.6, 130.5, 129.4, 129.2, 128.0, 128.2, 127.5, 126.5, 126.1, 125.8, 125.7, 125.2, 123.3, 122.8, 122.1, 121.1, 102.3, 74.3, 31.4, 26.4, 18.7. IR (KBr)  $\nu_{\max}/\text{cm}^{-1}$ : 3405, 3061, 2977, 2929, 1588, 1518, 1257, 1121, and 1054. HRMS (ESI-TOF) calculated for C<sub>26</sub>H<sub>22</sub>N<sub>2</sub>O<sub>2</sub> [M+H]<sup>+</sup>: 378.1732. Found: 379.1802, Figure S3.

#### Synthesis of 4,5-dihydro-6,6-dimethyl-6*H*-2-(4-hydroxyphenyl)-pyran[*b*-4,3]naphth[1,2-*d*]imidazole (**IM4**)

The reaction was heated to 70 °C for 1.0 h. Compound **IM4** was obtained as a gray amorphous solid (34 mg, 0.099 mmol, yield: 9.9%). <sup>1</sup>H NMR (400 MHz, DMSO-*d*<sub>6</sub>) δ [ppm]: 12.97 (s, 0.3H), 12.49 (s, 0.5H), 9.85 (s, 1H), 8.32–8.41 (m, 1H), 8.13 (d, 1H), 8.08 (d, 2H), 7.49–7.59 (m, 1H), 7.33–7.44 (m, 1H), 6.92 (d, *J* = 8.2 Hz, 2H), 2.96–3.14 (m, 2H), 1.89–1.98 (m, 2H), 1.42 (s, 6H). <sup>13</sup>C NMR (100 MHz, DMSO-*d*<sub>6</sub>) δ [ppm]: 158.3, 148.4, 143.9, 131.9, 130.7, 127.5, 125.5, 125.4, 123.0, 121.9, 121.9, 121.7, 121.0, 115.4, 102.3, 74.1, 31.3, 26.4, 18.7. IR (KBr)  $\nu_{\max}/\text{cm}^{-1}$ : 3422, 3071, 2974, 2849, 2929, 1613, 1533, 1265, 1160, and 1055. HRMS (ESI-TOF) calculated for C<sub>22</sub>H<sub>20</sub>N<sub>2</sub>O<sub>2</sub> [M+H]<sup>+</sup>: 345.1558. Found: 345.1590, Figure S4.

#### Synthesis of 4,5-dihydro-6,6-dimethyl-6*H*-2-(4-dimethylaminophenyl)-pyran[*b*-4,3]naphth[1,2-*d*]imidazole (**IM5**)

The reaction was heated to 70 °C for 3.0 h. Compound **IM5** was obtained as a light-yellow solid (121 mg, 0.326 mmol, yield: 32.6%), mp: 182–184 °C. <sup>1</sup>H NMR (400 MHz, DMSO-*d*<sub>6</sub>) δ [ppm]: 12.87 (s, 0.4H), 12.42 (s, 0.5H), 8.30–8.42 (m, 1H), 8.03–8.17 (m, 3H),

7.53 (t,  $J = 7.3$  Hz, 1H), 7.38 (t,  $J = 7.6$  Hz, 1H), 6.86 (d,  $J = 8.7$  Hz, 2H), 2.95–3.14 (m, 8H), 1.93–2.01 (m, 2H), 1.41 (s, 6H).  $^{13}\text{C}$  NMR (100 MHz, DMSO- $d_6$ )  $\delta$  [ppm]: 150.7, 150.6, 143.8, 130.8, 127.1, 125.5, 123.0, 122.4, 122.1, 121.2, 120.3, 112.0, 102.5, 74.1, 40.0, 31.5, 26.5, 18.9. IR (KBr)  $\nu_{\text{max}}/\text{cm}^{-1}$ : 3432, 3067, 2979, 2841, 2930, 1610, 1518, 1256, 1159, and 1055. HRMS (ESI-TOF) calculated for  $\text{C}_{24}\text{H}_{25}\text{N}_3\text{O}$   $[\text{M}+\text{H}]^+$ : 372.2031. Found: 372.2073, Figure S5.

#### Synthesis of 4,5-dihydro-6,6-dimethyl-6H-2-(4-nitrophenyl)-pyran[*b*-4,3]naphth[1,2-*d*]imidazole (**IM6**)

The reaction was heated to 70 °C for 30 min. Compound **IM6** was obtained as a red crystalline solid (183 mg, 0.490 mmol, yield: 49.1%), mp: 259–260 °C.  $^1\text{H}$  NMR (400 MHz, DMSO- $d_6$ )  $\delta$  [ppm]: 13.61 (s, 0.3H), 13.10 (s, 0.6H), 8.36–8.52 (m, 5H), 8.13–8.22 (m, 1H), 7.56–7.67 (m, 1H), 2.96–3.16 (m, 2H), 1.90–2.09 (m, 2H), 1.42, 144 (s, 6H).  $^{13}\text{C}$  NMR (100 MHz, DMSO- $d_6$ )  $\delta$  [ppm]: 146.8, 146.6, 144.2, 136.6, 133.0, 132.1, 126.6, 126.3, 125.7, 124.3, 124.0, 123.2, 122.3, 121.2, 102.2, 74.7, 31.3, 26.5, 18.7. IR (KBr)  $\nu_{\text{max}}/\text{cm}^{-1}$ : 3348, 2975, 2845, 2929, 1604, 1511, 1258, 1155, and 1057. HRMS (ESI-TOF) calculated for  $\text{C}_{22}\text{H}_{19}\text{N}_3\text{O}_3$   $[\text{M}+\text{H}]^+$ : 374.1460. Found: 374.1511, Figure S6.

#### Synthesis of 4,5-dihydro-6,6-dimethyl-6H-2-(2-nitrophenyl)-pyran[*b*-4,3]naphth[1,2-*d*]imidazole (**IM7**)

The reaction was heated to 70 °C for 2.5 h. Compound **IM7** was obtained as a red solid (194 mg, 0.520 mmol, yield: 52.0%), mp: 139–141 °C.  $^1\text{H}$  NMR (400 MHz, DMSO- $d_6$ )  $\delta$  [ppm]: 13.52 (s, 0.3H), 13.08 (s, 0.7H), 8.27 (d, 1H), 8.20–8.11 (m, 1H), 8.03 (t,  $J = 8.7$  Hz, 2H), 7.83–7.92 (m, 1H), 7.68–7.77 (m, 1H), 7.53–7.63 (m, 1H), 7.41–7.50 (m, 1H), 2.99 (t,  $J = 6.5$  Hz, 2H), 1.99 (t,  $J = 6.6$  Hz, 2H), 1.43, 1.41 (s, 6H).  $^{13}\text{C}$  NMR (100 MHz, DMSO- $d_6$ )  $\delta$  [ppm]: 148.8, 144.7, 143.8, 132.4, 132.6, 131.2, 130.9, 130.3, 126.1, 125.6, 124.6, 124.4, 123.7, 123.2, 122.2, 121.1, 102.2, 74.6, 31.4, 26.5, 18.7. IR (KBr)  $\nu_{\text{max}}/\text{cm}^{-1}$ : 3415, 3116, 2973, 2850, 2923, 1602, 1521, 1260, 1162, and 1057. HRMS (ESI-TOF) calculated for  $\text{C}_{22}\text{H}_{19}\text{N}_3\text{O}_3$   $[\text{M}+\text{H}]^+$ : 374.1460. Found: 374.1495, Figure S7.

### 3.3. Evaluation of Photophysical Properties

#### 3.3.1. Obtaining Visible Ultraviolet Absorption Spectra

A stock solution in dichloromethane ( $\text{CH}_2\text{Cl}_2$ ) of each compound was prepared at a concentration of 4000  $\mu\text{M}$ . From the stock solution, solutions were prepared at a concentration of 20  $\mu\text{M}$  of each compound in four different solvents: hexane,  $\text{CH}_2\text{Cl}_2$ , dimethyl sulfoxide (DMSO), and methanol ( $\text{CH}_3\text{OH}$ ). Then, measurement in the range of 190 to 800 nm was performed, with the wavelengths of maximum absorption ( $\lambda_{\text{max}}$ ) of the compounds in the different solvents shown in Table S1 and Figure S8.

#### 3.3.2. Molar Absorptivity Coefficient

The molar absorptivity coefficient ( $\epsilon_{\text{Abs}}$ ) was determined using an equation applied by Lambert–Beer ( $\epsilon_{\text{Abs}} = A/L \times C$ , where  $A$ —maximum absorbance;  $L$ —the optical path of the cuvette used (1 cm); and  $C$ —concentration of the analyzed sample in M).

#### 3.3.3. Fluorescence Emission Spectrum and Stokes Shift

Stock solutions used for each compound, at a concentration of 4000  $\mu\text{M}$ , in the solvents in which the sample showed better resolution of the maximum absorption band, were DMSO for **IM2**,  $\text{CH}_3\text{OH}$  for **IM6**, hexane for **IM7**, and  $\text{CH}_2\text{Cl}_2$  for the others. The stock solutions were diluted to a concentration of 20  $\mu\text{M}$ , and readings used the excitation wavelength of 345 nm for all compounds. The Stokes shift ( $\Delta\sigma_{\text{T}}$ ) was calculated from the difference between the absorbance and excitation wavelengths ( $\lambda_{\text{Abs}} - \lambda_{\text{Emis}}$ ), Figure S8.

### 3.4. Evaluation of the Cytotoxic Activity

#### 3.4.1. Cell Lines

Brain tumor (SNB-19), human colorectal carcinoma (HCT-116), and human promyelocytic leukemia (HL-60) cells were obtained from the National Cancer Institute (NCI) (Bethesda, MD, USA). The L929 cells (mouse fibroblast L cells NCTC clone 929) were purchased from the American Type Culture Collection (Manassas, VA, USA). The cells were grown on RPMI 1640 medium supplemented with 10% fetal bovine serum and 1% antibiotics (penicillin/streptomycin) at 37 °C with 5% CO<sub>2</sub>.

#### 3.4.2. Assessment of In Vitro Anticancer Activity

Cytotoxic potential of the naphth[1,2-*d*]imidazoles **IM1–IM7** was assessed after 72 h of exposure to the tumor cell lines of human SNB-19, HCT-116, HL-60, and normal cell line L929. Cells were plated in 96-well plates ( $0.7 \times 10^5$  cells/well for SNB-19,  $0.3 \times 10^6$  cells/well for HCT-116, and  $0.3 \times 10^6$  cells/well for HL-60). Compounds were dissolved with DMSO at concentrations in the 0.078–10 µg.mL<sup>-1</sup> range. Doxorubicin (0.001–1.10 µM) was used as the positive control, and negative control groups received the same amount of vehicle (DMSO). The cell viability was determined by the reduction of the yellow dye 3-(4,5-dimethyl-2-thiazol)-2,5-diphenyl-2H-tetrazolium bromide (MTT) to a blue formazan product [35]. At the end of the incubation time (69 h), the plates were centrifuged, and the medium was replaced with fresh medium (200 µL) containing 0.5 mg/mL of MTT. Three hours later, the MTT formazan product was dissolved in DMSO (150 µL), and the absorbance was measured using a multi-plate reader (Spectra Count, Packard, ON, Canada). The drug effect was quantified as the percentage of control absorbance of the reduced dye at 550 nm. All experiments were performed in three independent assays, and the half maximal inhibitory concentration (IC<sub>50</sub>) and their 95% confidence intervals were achieved by nonlinear regression.

## 4. Conclusions

Naphth[1,2-*d*]imidazoles **IM1–IM7** showed high levels of cytotoxic activity and selectivity against the tested cancer cells and promising optical properties. The cytotoxicity results and photophysical properties presented by naphth[1,2-*d*]imidazoles **IM2**, **IM3**, **IM4**, and **IM5** qualify them for further studies in the development of fluorescent anticancer probes using this scaffold, making possible the use of naphth[1,2-*d*]imidazoles as fluorescent probes/therapeutic molecules in theranostic systems for cancer treatment/diagnosis.

**Supplementary Materials:** The following supporting information can be downloaded at <https://www.mdpi.com/article/10.3390/molecules28073008/s1>. Figure S1: NMR spectra of 4,5-dihydro-6,6-dimethyl-6H-2-pyran[*b*-4,3]naphth[1,2-*d*]imidazole (**IM1**) in DMSO-*d*<sub>6</sub>; Figure S2: NMR spectra of 4,5-dihydro-6,6-dimethyl-6H-2-(phenyl)-pyran[*b*-4,3]naphth[1,2-*d*]imidazole (**IM2**) in DMSO-*d*<sub>6</sub> and ESI-MS; Figure S3: NMR spectra of 4,5-dihydro-6,6-dimethyl-6H-2-(naphthalenyl)-pyran[*b*-4,3]naphth[1,2-*d*]imidazole (**IM3**) in DMSO-*d*<sub>6</sub> and ESI-MS; Figure S4: NMR spectra of 4,5-dihydro-6,6-dimethyl-6H-2-(4-hydroxyphenyl)-pyran[*b*-4,3]naphth[1,2-*d*]imidazole (**IM4**) in DMSO-*d*<sub>6</sub> and ESI-MS; Figure S5: NMR spectra of 4,5-dihydro-6,6-dimethyl-6H-2-(4-dimethylaminophenyl)-pyran[*b*-4,3]naphth[1,2-*d*]imidazole (**IM5**) in DMSO-*d*<sub>6</sub> and ESI-MS; Figure S6: NMR spectra of 4,5-dihydro-6,6-dimethyl-6H-2-(4-nitrophenyl)-pyran[*b*-4,3]naphth[1,2-*d*]imidazole (**IM6**) in DMSO-*d*<sub>6</sub> and ESI-MS; Figure S7: NMR spectra of 4,5-dihydro-6,6-dimethyl-6H-2-(2-nitrophenyl)-pyran[*b*-4,3]naphth[1,2-*d*]imidazole (**IM7**) in DMSO-*d*<sub>6</sub> and ESI-MS; Figure S8: Absorbance and emission spectra of naphthoimidazoles **IM1–IM7**; Table S1: Wavelength (nm) and absorbance of the scanning spectra of the naphth[1,2-*d*]imidazoles obtained in the solvatochromism study.

**Author Contributions:** Conceptualization, V.L.d.A.S., H.P.d.O., C.P. and C.R.M.A.; formal analysis, V.L.d.A.S., A.d.A.G., M.P.d.C., F.d.C.E.d.O. and C.R.M.A.; funding acquisition, H.P.d.O., C.P. and C.R.M.A.; investigation, V.L.d.A.S., D.G.G., S.S.S. and L.P.S.R.; methodology, V.L.d.A.S., H.P.d.O., M.P.d.C. and F.d.C.E.d.O.; project administration, C.R.M.A.; writing—original draft, V.L.d.A.S. and C.R.M.A.; writing—review and editing, A.d.A.G., M.P.d.C. and C.R.M.A. All authors have read and agreed to the published version of the manuscript.

**Funding:** This research received funding from the Coordination of the Improvement of Higher Education Personnel (CAPES), Brazil, process no. 88881.708019/2022-01 of the PDPG-consolidação-3-4 program and Research Support Foundation of Pernambuco (FACEPE)—process no. IBPG-0457-1.06/20.

**Institutional Review Board Statement:** Not applicable.

**Informed Consent Statement:** Not applicable.

**Data Availability Statement:** Data is contained within the article or Supplementary Material.

**Acknowledgments:** We are grateful to the following Brazilian agencies: Coordination of the Improvement of Higher Education Personnel (CAPES) and Research Support Foundation of Pernambuco (FACEPE).

**Conflicts of Interest:** The authors declare that they have no known competing financial interests or personal relationships that could have influenced the work reported in this paper.

**Sample Availability:** Samples of the compounds are available from the authors.

## References

1. Kelkar, S.S.; Reineke, T.M. Theranostics: Combining Imaging and Therapy. *Bioconjugate Chem.* **2011**, *22*, 1879–1903. [[CrossRef](#)]
2. Xiao, S.; Tang, Y.; Lv, Z.; Lin, Y.; Chen, L. Nanomedicine—Advantages for their use in rheumatoid arthritis theranostics. *J. Control. Release* **2019**, *316*, 302–316. [[CrossRef](#)] [[PubMed](#)]
3. Golovin, Y.; Klyachko, N.; Majouga, A.; Kabanov, A. Modeling drug release from functionalized magnetic nanoparticles actuated by non-heating low frequency magnetic field. *J. Nanoparticle Res.* **2017**, *64*, 19. [[CrossRef](#)]
4. Jain, T.; Kumar, S.; Dutta, P.K. Theranostics: A Way of Modern Medical Diagnostics and the Role of Chitosan. *J. Mol. Genet. Med.* **2014**, *9*, 1000159. [[CrossRef](#)]
5. Cole, J.T.; Holland, N.B. Multifunctional nanoparticles for use in theranostic applications. *Drug Deliv. Transl. Res.* **2015**, *5*, 295–309. [[CrossRef](#)]
6. Santos, V.; Guimarães, D.; Nishimura, R.; Rolim, L.; Gonsalves, A.; Araújo, C. Naftoimidazóis e naftoxazóis—Promissores componentes de sistemas teranósticos. *Quim. Nova* **2022**, *45*, 560–577. [[CrossRef](#)]
7. Kerru, N.; Bhaskaruni, S.V.H.S.; Gummidi, L.; Maddila, S.N.; Maddila, S.; Jonnalagadda, S.B. Recent advances in heterogeneous catalysts for the synthesis of imidazole derivatives. *Synth. Commun.* **2019**, *49*, 2437–2459. [[CrossRef](#)]
8. Santos, V.; Gonsalves, A.; Araújo, C. Resgate da reação de debus-radziszewski: Ensino prático de reações multicomponentes na síntese da lofina. *Quim. Nova* **2020**, *43*, 1344–1349. [[CrossRef](#)]
9. Bombaça, A.C.S.; Silva, L.A.; Chaves, O.A.; da Silva, L.S.; Barbosa, J.M.; da Silva, A.M.; Ferreira, A.B.; Menna-Barreto, R.F. Novel N,N-di-alkyl-naphthoimidazolium derivative of  $\beta$ -lapachone impaired *Trypanosoma cruzi* mitochondrial electron transport system. *Biomed. Pharmacother.* **2021**, *135*, 111186. [[CrossRef](#)]
10. Moura, K.C.; Carneiro, P.F.; Pinto, M.D.C.F.; da Silva, J.A.; Malta, V.; de Simone, C.A.; Dias, G.; Jardim, G.A.; Cantos, J.; Coelho, T.S.; et al. 1,3-Azoles from ortho-naphthoquinones: Synthesis of aryl substituted imidazoles and oxazoles and their potent activity against *Mycobacterium tuberculosis*. *Bioorganic Med. Chem.* **2012**, *20*, 6482–6488. [[CrossRef](#)]
11. Castellanos, J.R.G.; Prieto, J.M.; Heinrich, M. Red Lapacho (*Tabebuia impetiginosa*)—A global ethnopharmacological commodity? *J. Ethnopharmacol.* **2009**, *121*, 1–13. [[CrossRef](#)] [[PubMed](#)]
12. Moon, D.-O.; Kang, C.-H.; Kim, M.-O.; Jeon, Y.-J.; Lee, J.-D.; Choi, Y.H.; Kim, G.-Y.  $\beta$ -Lapachone (LAPA) Decreases Cell Viability and Telomerase Activity in Leukemia Cells: Suppression of Telomerase Activity by LAPA. *J. Med. Food* **2010**, *13*, 481–488. [[CrossRef](#)] [[PubMed](#)]
13. Jardim, G.A.M.; Lima, D.J.B.; Valença, W.O.; Cavalcanti, B.C.; Pessoa, C.; Rafique, J.; Braga, A.L.; Jacob, C.; Da Silva Júnior, E.N.; Da Cruz, E.H.G. Synthesis of Selenium-Quinone Hybrid Compounds with Potential Antitumor Activity via Rh-Catalyzed C-H Bond Activation and Click Reactions. *Molecules* **2017**, *23*, 83. [[CrossRef](#)] [[PubMed](#)]
14. Costa, D.C.F.; Rangel, L.P.; Martins-Dinis, M.M.D.C.; Ferretti, G.D.S.; Ferreira, V.F.; Silva, J.L. Anticancer potential of resveratrol,  $\beta$ -lapachone and their analogues. *Molecules* **2020**, *25*, 893. [[CrossRef](#)]
15. Khong, H.T.; Dreisbach, L.; Kindler, H.L.; Trent, D.F.; Jeziorski, K.G.; Bonderenko, I.; Popiela, T.; Yagovane, D.M.; Dombal, G. A phase 2 study of ARQ 501 in combination with gemcitabine in adult patients with treatment naïve, unresectable pancreatic adenocarcinoma. *J. Clin. Oncol.* **2007**, *25*, 15017. [[CrossRef](#)]
16. Kawecki, A.; Adkins, D.R.; Cunningham, C.C.; Vokes, E.; Yagovane, D.M.; Dombal, G.; Koralewski, P.; Hotko, Y.; Vladimirov, V. A phase II study of ARQ 501 in patients with advanced squamous cell carcinoma of the head and neck. *J. Clin. Oncol.* **2007**, *25*, 16509. [[CrossRef](#)]
17. Gerber, D.E.; Beg, M.S.; Fattah, F.; Frankel, A.E.; Fatunde, O.; Arriaga, Y.; Dowell, J.E.; Bisen, A.; Leff, R.D.; Meek, C.C.; et al. Phase 1 study of ARQ 761, a  $\beta$ -lapachone analogue that promotes NQO1-mediated programmed cancer cell necrosis. *Br. J. Cancer* **2018**, *119*, 928–936. [[CrossRef](#)]

18. Kim, S.; Lee, S.; Cho, J.-Y.; Yoon, S.H.; Jang, I.-J.; Yu, K.-S. Pharmacokinetics and tolerability of MB12066, a beta-lapachone derivative targeting NAD(P)H:quinone oxidoreductase 1: Two independent, double-blind, placebo-controlled, combined single and multiple ascending dose first-in-human clinical trials. *Drug Des. Dev. Ther.* **2017**, *11*, 3187–3195. [[CrossRef](#)]
19. Kim, I.; Kim, H.; Ro, J.; Jo, K.; Karki, S.; Khadka, P.; Yun, G.; Lee, J. Preclinical Pharmacokinetic Evaluation of  $\beta$ -Lapachone: Characteristics of Oral Bioavailability and First-Pass Metabolism in Rats. *Biomol. Ther.* **2015**, *23*, 296–300. [[CrossRef](#)] [[PubMed](#)]
20. Blanco, E.; Bey, E.A.; Khemtong, C.; Yang, S.-G.; Setti-Guthi, J.; Chen, H.; Kessinger, C.W.; Carnevale, K.A.; Bornmann, W.G.; Boothman, D.A.; et al.  $\beta$ -Lapachone Micellar Nanotherapeutics for Non-Small Cell Lung Cancer Therapy. *Cancer Res* **2010**, *70*, 3896–3904. [[CrossRef](#)]
21. Pavoni, J.; Neves-Junior, W.; Spiropulos, M.; De Araujo, D. Uma montagem experimental para a medida de fluorescência. *Rev. Bras. de Ensino de Física* **2014**, *36*, 1–9. [[CrossRef](#)]
22. Bozkurt, E.; Dogan, S.D. Photophysical behavior of a novel 4-aza-indole derivative in different solvents: Reverse solvatochromism. *Res. Chem. Intermed.* **2018**, *45*, 863–872. [[CrossRef](#)]
23. de Rezende, L.C.D.; Vaidergorn, M.M.; Moraes, J.C.B.; Emery, F.D.S. Synthesis, Photophysical Properties and Solvatochromism of Meso-Substituted Tetramethyl BODIPY Dyes. *J. Fluoresc.* **2013**, *24*, 257–266. [[CrossRef](#)] [[PubMed](#)]
24. Telegin, F.Y.; Marfin, Y.S. New insights into quantifying the solvatochromism of BODIPY based fluorescent probes. *Spectrochim. Acta Part A Mol. Biomol. Spectrosc.* **2021**, *255*, 119683. [[CrossRef](#)]
25. Chen, S.; Hong, F. Palladium-Catalyzed C-H Functionalization of Amido-Substituted 1,4-Naphthoquinone in the Presence of Amines toward the Formation of Pyrroles and Imidazoles. *Chemistryselect* **2017**, *2*, 10232–10238. [[CrossRef](#)]
26. Nagarajan, N.; Vanitha, G.; Ananth, D.A.; Rameshkumar, A.; Sivasudha, T.; Renganathan, R. Bioimaging, antibacterial and antifungal properties of imidazole-pyridine fluorophores: Synthesis, characterization and solvatochromism. *J. Photochem. Photobiol. B: Biol.* **2013**, *127*, 212–222. [[CrossRef](#)]
27. De Souza, V.P.; Vendrusculo, V.; Morás, A.M.; Steffens, L.; Santos, F.S.; Moura, D.J.; Rodembusch, F.S.; Russowsky, D. Synthesis and photophysical study of new fluorescent proton transfer dihydropyrimidinone hybrids as potential candidates for molecular probes. *New J. Chem.* **2017**, *41*, 15305–15311. [[CrossRef](#)]
28. Valeur, B.; Berberan-Santos, M.N. *Molecular fluorescence: Principles and applications*, 2nd ed.; John Wiley & Sons: Weinheim, Germany, 2012.
29. Liu, X.; Xu, Z.; Cole, J.M. Molecular Design of UV-vis Absorption and Emission Properties in Organic Fluorophores: Toward Larger Bathochromic Shifts, Enhanced Molar Extinction Coefficients, and Greater Stokes Shifts. *J. Phys. Chem. C* **2013**, *117*, 16584–16595. [[CrossRef](#)]
30. Tariq, A.; Garnier, U.; Ghasemi, R.; Lefevre, J.P.; Mongin, C.; Brosseau, A.; Audibert, J.F.; Pansu, R.; Dauzères, A.; Leray, I. Perylene based PET fluorescent molecular probes for pH monitoring. *J. Photochem. Photobiol. A Chem.* **2022**, *432*, 114035. [[CrossRef](#)]
31. Ghodbane, A.; Colléaux, J.; Saffon, N.; Mahiou, R.; Galaup, J.-P.; Fery-Forgues, S. Blue-Emitting Nanocrystals, Microcrystals, and Highly Oriented Nanofibers Prepared by Reprecipitation and Solvent Drop-Casting of 2-Phenyl-naphthoxazoles. *Chempluschem* **2012**, *78*, 185–191. [[CrossRef](#)]
32. Farahat, A.A.; Kumar, A.; Say, M.; Wenzler, T.; Brun, R.; Paul, A.; Wilson, W.D.; Boykin, D.W. Exploration of DAPI analogues: Synthesis, antitrypanosomal activity, DNA binding and fluorescence properties. *Eur. J. Med. Chem.* **2017**, *128*, 70–78. [[CrossRef](#)] [[PubMed](#)]
33. Dođru, Ü.; Ürüt, G.; Bayramin, D. Synthesis and spectroscopic characterization of Y-shaped fluorophores with an imidazole core containing crown ether moieties. *J. Lumin.* **2015**, *163*, 32–39. [[CrossRef](#)]
34. Chipem, F.A.S.; Mishra, A.; Krishnamoorthy, G. The role of hydrogen bonding in excited state intramolecular charge transfer. *Phys. Chem. Chem. Phys.* **2012**, *14*, 8775–8790. [[CrossRef](#)]
35. Liu, T.; Zhang, J.; Cao, J.; Zheng, H.; Zhan, C.; Liu, H.; Zhang, L.; Xiao, K.; Liu, S.; Xiang, D.; et al. Identification of coexistence of biological and non-biological aerosol particles with DAPI (4',6-diamidino-2-phenylindole) stain. *Particuology* **2023**, *72*, 49–57. [[CrossRef](#)]
36. Hu, J.; Guo, Y.; Geng, X.; Wang, J.; Li, S.; Sun, Y.; Qu, L.; Li, Z. Tuning asymmetric electronic structure endows carbon dots with unexpected huge stokes shift for high contrast in vivo imaging. *Chem. Eng. J.* **2022**, *446*, 136928. [[CrossRef](#)]
37. Araneda, J.F.; Piers, W.E.; Heyne, B.; Parvez, M.; McDonald, R. High Stokes Shift Anilido-Pyridine Boron Difluoride Dyes. *Angew. Chem. Int. Ed.* **2011**, *50*, 12214–12217. [[CrossRef](#)]
38. Shcherbakova, D.M.; Hink, M.A.; Joosen, L.; Gadella, T.W.J.; Verkhusha, V.V. An Orange Fluorescent Protein with a Large Stokes Shift for Single-Excitation Multicolor FCCS and FRET Imaging. *J. Am. Chem. Soc.* **2012**, *134*, 7913–7923. [[CrossRef](#)] [[PubMed](#)]
39. Wu, X.; Sun, X.; Guo, Z.; Tang, J.; Shen, Y.; James, T.D.; Tian, H.; Zhu, W. *In Vivo* and *in Situ* Tracking Cancer Chemotherapy by Highly Photostable NIR Fluorescent Theranostic Prodrug. *J. Am. Chem. Soc.* **2014**, *136*, 3579–3588. [[CrossRef](#)] [[PubMed](#)]
40. Wu, I.-C.; Yu, J.; Ye, F.; Rong, Y.; Gallina, M.E.; Fujimoto, B.S.; Zhang, Y.; Chan, Y.-H.; Sun, W.; Zhou, X.-H.; et al. Squaraine-Based Polymer Dots with Narrow, Bright Near-Infrared Fluorescence for Biological Applications. *J. Am. Chem. Soc.* **2014**, *137*, 173–178. [[CrossRef](#)] [[PubMed](#)]
41. Mosmann, T. Rapid colorimetric assay for cellular growth and survival: Application to proliferation and cytotoxicity assays. *J. Immunol. Methods* **1983**, *65*, 55–63. [[CrossRef](#)]

42. Peña-Morán, O.A.; Villarreal, M.L.; Álvarez-Berber, L.; Meneses-Acosta, A.; Rodríguez-López, V. Cytotoxicity, Post-Treatment Recovery, and Selectivity Analysis of Naturally Occurring Podophyllotoxins from *Bursera fagaroides* var. *fagaroides* on Breast Cancer Cell Lines. *Molecules* **2016**, *21*, 1013. [[CrossRef](#)] [[PubMed](#)]
43. Zhang, J.; Chen, R.; Zhu, Z.; Adachi, C.; Zhang, X.; Lee, C.-S. Highly Stable Near-Infrared Fluorescent Organic Nanoparticles with a Large Stokes Shift for Noninvasive Long-Term Cellular Imaging. *ACS Appl. Mater. Interfaces* **2015**, *7*, 26266–26274. [[CrossRef](#)] [[PubMed](#)]
44. Souza, M.A.A.D.; Silva, A.R.D.; Ferreira, M.A.; Lemos, M.J.D.; Ramos, R.G.; Ferreira, A.B.B.; Souza, S.R.D. Atividade biológica do lapachol e de alguns derivados sobre o desenvolvimento fúngico e em germinação de sementes. *Quim. Nova* **2008**, *31*, 1670–1672. [[CrossRef](#)]
45. Yu, D.; Chen, X.-L.; Ai, B.-R.; Zhang, X.-M.; Wang, J.-Y. Tetrabutylammonium iodide catalyzed hydroxylation of naphthoquinone derivatives with tert-butyl hydroperoxide as an oxidant. *Tetrahedron Lett.* **2018**, *59*, 3620–3623. [[CrossRef](#)]
46. Singh, P.; Natani, K.; Jain, S.; Arya, K.; Dandia, A. Microwave-assisted rapid cyclization of lapachol, a main constituent of *Heterophragma adenophyllum*. *Nat. Prod. Res.* **2006**, *20*, 207–212. [[CrossRef](#)] [[PubMed](#)]

**Disclaimer/Publisher's Note:** The statements, opinions and data contained in all publications are solely those of the individual author(s) and contributor(s) and not of MDPI and/or the editor(s). MDPI and/or the editor(s) disclaim responsibility for any injury to people or property resulting from any ideas, methods, instructions or products referred to in the content.